Rapid curing dynamics of PEG-thiol-ene resins allow facile 3D bioprinting and in-air cell-laden microgel fabrication

Jang, Lindy K.
Ahlquist, Jesse
Ye, Congwang
Trujillo, Juliana
Triplett, Michael
Moya, Monica L.
Robertson, Claire J.
Hynes, William F.
Wasson, Elisa M.

To be published in: Biomedical Materials

DOI to publisher's version: 10.1088/1748-605X/ad8540

Biomedical Materials

PAPER • **OPEN ACCESS**

Rapid curing dynamics of PEG-thiol-ene resins allow facile 3D bioprinting and in-air cell-laden microgel fabrication

To cite this article: Lindy K Jang *et al* 2025 *Biomed. Mater.* **20** 015009

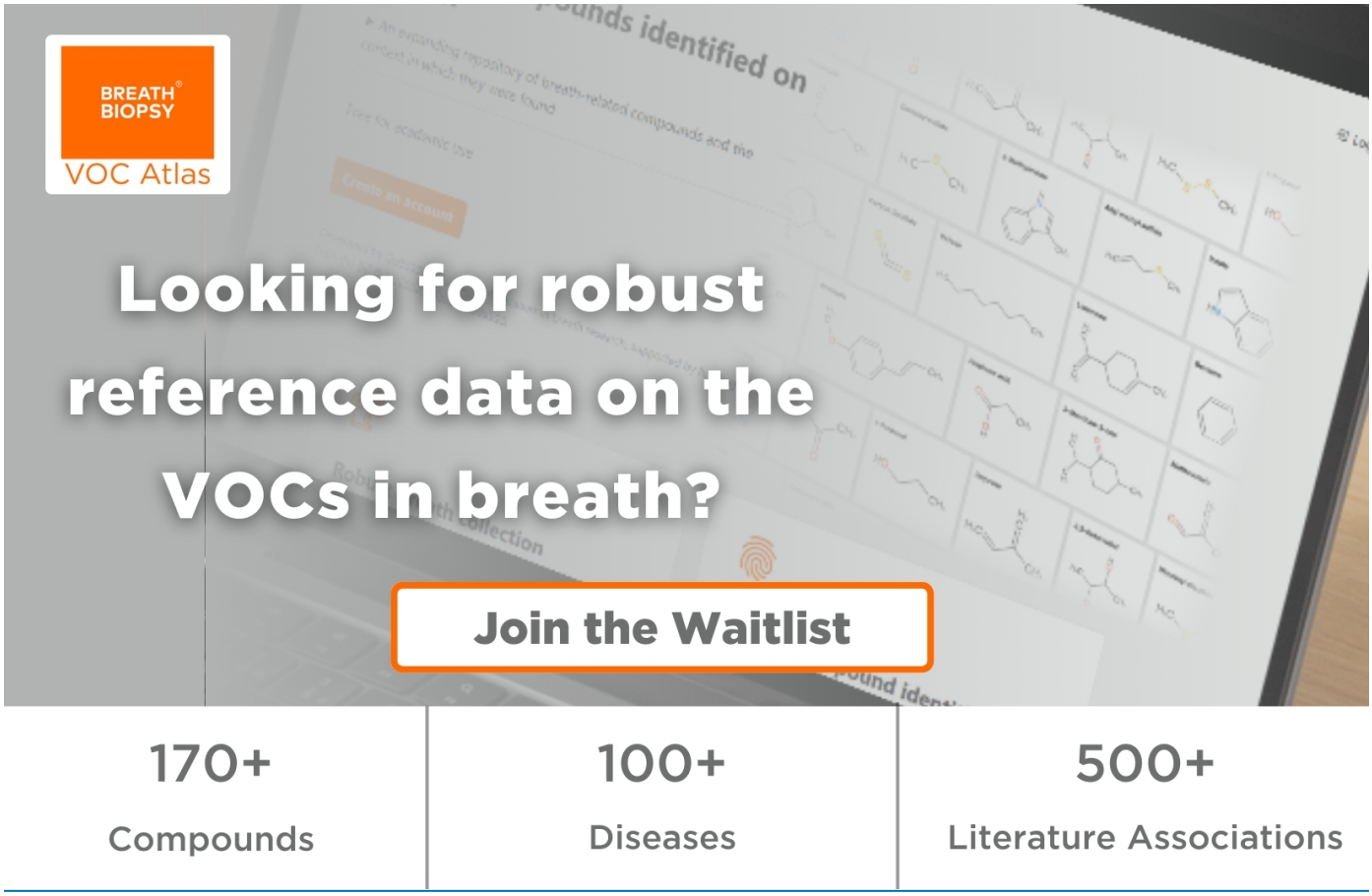

IOP Publishing Biomed. Mater. 20 (2025) 015009 https://doi.org/10.1088/1748-605X/ad8540

Biomedical Materials

OPEN ACCESS

RECEIVED
20 May 2024

REVISED
6 August 2024

ACCEPTED FOR PUBLICATION
9 October 2024

PUBLISHED
25 November 2024

PAPER

Rapid curing dynamics of PEG-thiol-ene resins allow facile 3D bioprinting and in-air cell-laden microgel fabrication

Lindy K Jang[1], Jesse T Ahlquist[1], Congwang Ye[1], Juliana Trujillo[2], Michael Triplett[1], Monica L Moya[1], Claire Robertson[1,4], William Hynes[1,5] and Elisa M Wasson[1,3,5,*]

[1] Materials Engineering Division, Lawrence Livermore National Laboratory, Livermore, CA, United States of America
[2] Department of Biomedical Engineering, University of Virginia, Charlottesville, VA, United States of America
[3] Bioscience Division, Los Alamos National Laboratory, Los Alamos, NM, United States of America
[4] UC Davis Comprehensive Cancer Center, Davis, CA, United States of America
[5] Indicates co-senior authors.
[*] Author to whom any correspondence should be addressed.

E-mail: ewasson@lanl.gov

Keywords: microgel, cell encapsulation, in-air photopolymerization, 3D printing, bioprinting, tissue engineering, bioresin

Supplementary material for this article is available online

Abstract

Thiol-norbornene photoclick hydrogels are highly efficient in tissue engineering applications due to their fast gelation, cytocompatibility, and tunability. In this work, we utilized the advantageous features of polyethylene glycol (PEG)-thiol-ene resins to enable fabrication of complex and heterogeneous tissue scaffolds using 3D bioprinting and in-air drop encapsulation techniques. We demonstrated that photoclickable PEG-thiol-ene resins could be tuned by varying the ratio of PEG-dithiol to PEG norbornene to generate a wide range of mechanical stiffness (0.5–12 kPa) and swelling ratios. Importantly, all formulations maintained a constant, rapid gelation time (<0.5 s). We used this resin in biological projection microstereolithography (BioPμSL) to print complex structures with geometric fidelity and demonstrated biocompatibility by printing cell-laden microgrids. Moreover, the rapid gelling kinetics of this resin permitted high-throughput fabrication of tunable, cell-laden microgels in air using a biological in-air drop encapsulation apparatus (BioIDEA). We demonstrated that these microgels could support cell viability and be assembled into a gradient structure. This PEG-thiol-ene resin, along with BioPμSL and BioIDEA technology, will allow rapid fabrication of complex and heterogeneous tissues that mimic native tissues with cellular and mechanical gradients. The engineered tissue scaffolds with a controlled microscale porosity could be utilized in applications including gradient tissue engineering, biosensing, and *in vitro* tissue models.

1. Introduction

Tissue engineering aims to fabricate functional tissue constructs that can facilitate regeneration of damaged tissues [1], serve as *in vitro* models for testing new drugs or medical devices, and aid in understanding physiological or pathological phenomena for diagnostic and therapeutic purposes [2]. A key challenge for tissue engineering is replicating the chemical, biological, and mechanical complexities of native tissues or organs. Tissues have complex three-dimensional (3D) architectures and cellular gradients of one or more cell types [3, 4]. Interface tissues like bone-cartilage interface have mechanical gradients and replicating the complexity of such tissues remains as a major tissue engineering challenge. Therefore, versatile, biocompatible scaffold materials and biofabrication technologies are needed to recapitulate the complexity of native tissues and construct functional biomimetic tissue structures [5].

Various biofabrication approaches have been introduced to mimic the complexity of natural tissues *in vivo* [6–9]. Photopolymerization methods, which crosslink hydrogels by light, enable fabrication of tissue scaffolds through a variety of approaches including 3D printing and fabrication of micrometer-sized hydrogels, or microgels [10–13].

Digital light processing (DLP) 3D bioprinting can readily print high-resolution tissue scaffolds (∼50 μm feature size) with rapid printing speed without exerting shear stress on encapsulated cells [14, 15]. Polyethylene glycol diacrylate (PEGDA) hydrogels can be printed with DLP printing into complex shaped implants [16]. However, high concentrations of photoinitiator and high light exposure is required to achieve high printing accuracy, which can decrease cell viability. Although many acrylate based hydrogel resins have been investigated for use in DLP bioprinting [17–20], there is a crucial need for new DLP hydrogel resins.

As the field of biofabrication continues to evolve, complementary methods to traditional bioprinting are gaining prominence. Among these, microgel based tissue scaffolds offer a promising avenue for generating complex biomimetic tissue scaffolds in a modular fashion. Microgels with tunable size, mechanical stiffness, and biochemical properties serve as individual building blocks to fabricate porous tissue scaffolds that can mimic the heterogeneity of biological tissues [12, 21, 22]. We have recently developed an innovative in-air photopolymerization system called the in-air drop encapsulation apparatus (IDEA) [23], which improves greatly on microgel throughput over microfluidic synthesis approaches [24, 25]. This system fabricates microdroplets in the air by generating instabilities in a liquid jet ejected from a nozzle through vibration. The droplets are photopolymerized mid-air, achieving droplet formation up to 50–1000× faster than traditional microfluidics and without the need for a secondary shell, unlike other commercially available in-air systems that use photocurable materials [26, 27]. While Jiang *et al* previously fabricated microgels by photopolymerizing polymer droplets in air, they did so in the absence of cells, using high concentrations of PEGDA and other non biocompatible materials not suitable for cell encapsulation [28]. To the best of our knowledge, fabricating cell-laden microgels using the in-air photopolymerization technique has not been demonstrated to date. Developing biomaterials that can cure rapidly with controllable mechanical properties that enable the transport of nutrients to encapsulated cells remains a significant challenge for this microgel fabrication approach.

PEGDA materials are one of the most commonly used hydrogels for tissue engineering as they are mechanically tunable and highly reproducible [29], and a wide range of bioactive molecules can be incorporated into the hydrogels to serve specific biological functions [30]. Importantly, photopolymerization can readily occur at physiological temperature and pH [31, 32]. Although acrylate-based hydrogels offer high reactivity [33], acrylate macromers undergo radical mediated chain-growth polymerization which leads to a heterogeneous crosslinking network and high brittleness [34]. Oxygen inhibition is another limitation of acrylate polymerization especially when the materials are polymerized in open air [35]. In addition, crosslinking speed of PEGDA varies significantly depending on the molecular weight or the concentration of the macromer which makes it difficult to tune the mechanical properties using varying formulations under the same fabrication condition [36, 37].

Thiol-ene macromers, on the other hand, polymerize through step-growth mechanism which results in more homogeneous crosslinking networks and less brittle structure [34]. Compared to acrylate free radical polymerization, thiol-ene click chemistry offers faster reaction kinetics in mild reaction conditions, insensitivity to moisture and oxygen, lower concentration of photoinitiators required for the initiation step, and better cytocompatibility [38–41]. Among various thiol-ene reactions, the thiol-norbornene reaction is representative of a true step growth polymerization where no homopolymerization or chain growth is observed due to the high reactivity of electron-rich norbornenes [42, 43]. However, only limited studies have been conducted in characterizing thiol-norbornene based hydrogel resins in DLP bioprinting [44, 45] and in-air microgel fabrication.

In this work, we demonstrate that the unique properties of polyethylene glycol (PEG)-thiol-ene hydrogels are suitable for tissue engineering of complex structures using both DLP 3D bioprinting and in-air photopolymerized microgel fabrication. We utilized PEG dithiol and 8arm PEG norbornene in combination with lithium phenyl-2,4,6-trimethylbenzoylphosphinate (LAP) as a photoinitiator. Our study investigated the mechanical properties of PEG-thiol-ene hydrogels at various SH:NB ratios, concentrations of photoinitiator, or molecular weight of PEG-dithiol. We successfully 3D printed various high-resolution prints and fabricated microgels in the air with varying mechanical stiffness that could be used for tissue scaffolds. For the first time, we demonstrated cell encapsulation in microgels using our in-air photopolymerization system. Additionally, we assembled microgels to form a three-layered porous scaffold with a gradient in stiffness. By leveraging the advantageous properties of PEG thiol-ene hydrogels, we established a novel in-air cell laden microgel fabrication technique that may enable the scalable production of heterogeneous and complex cell-laden tissue scaffolds.

2. Materials and methods

2.1. Preparation of PEG-thiol-ene resins

PEG dithiol (3.5 kDa, A4001; 5 kDa, A4075) and 8arm PEG norbornene (20 kDa, A10037) were purchased from JenKem Technology USA. LAP (900889) and quinoline yellow (QY, 309052) were purchased from Sigma-Aldrich.

Stock solutions of 20 wt% 8arm PEG norbornene (PEG-NB, 20 kDa), 20 wt% PEG dithiol (PEG-SH, 3.5 kDa or 5 kDa), 1 wt% LAP, and 1 wt% QY were prepared by dissolving them in HBSS (for biological in-air drop encapsulation apparatus (BioIDEA) resin) or PBS (for biological projection microstereolithography (BioPμSL) resin) and vortexing them for 1 min to ensure homogeneity.

BioPμSL resin was prepared by mixing stock solutions to obtain a final concentration of 5 wt% PEG-NB (20 kDa), 10 wt% PEG-SH (5 kDa), 0.01 wt% LAP photoinitiator and 0.04 wt% QY photoabsorber.

Multiple resin formulations of BioIDEA were prepared by mixing stock solutions to obtain a final concentration of 5 wt% PEG-NB (20 kDa), 5–10 wt% PEG-SH (3.5 kDa), and 0.01–0.6 wt% LAP photoinitiator.

2.2. Characterization of PEG-thiol-ene hydrogels

2.2.1. PEG-thiol-ene formulations

Numerous formulations were explored to identify resins with suitable mechanical properties and curing kinetics necessary for bioprinting and in-air microgel fabrication. PEG-SH molecular weight and concentration, as well as photoinitiator concentration were varied to isolate their respective effects on modulus, swelling, and rapid curing properties.

2.2.2. Rheology of PEG-thiol-ene hydrogels

Dynamic shear oscillatory measurements were performed with a parallel plate rheometer equipped with a UV–Vis curing system (PP25, Anton Paar, MCR 103). Time sweeps were performed at 0.1% strain, 10 Hz frequency, 0.2 mm gap, and 23 °C. Uncured resins were loaded on to the rheometer and baseline measurements were taken for 30 s before being exposed to a 27 mW cm^{-2} light for 3 min at either 405 nm or 365 nm to simulate the 3D printing and in-air microgel fabrication techniques respectively. The reported storage modulus was calculated by averaging the storage modulus values at steady state. Gelation time was calculated as the time from initiation of light exposure to the point at which the storage modulus became higher than the loss modulus. Three replicate samples were measured for each resin condition.

2.2.3. Swelling of PEG-thiol-ene hydrogels

For swelling measurements of 3D printed hydrogels, three blocks (3 × 3 × 2 mm) were printed using BioPμSL and the blocks were swelled in PBS for 24 h. Dimensions of the prints were measured before and after swelling using an inverted microscope (Olympus IX3). The expansion ratio was calculated by dividing the final volume after swelling by the initial volume before swelling.

For each BioIDEA resin combination, three 10 µl droplets of uncured resin were pipetted onto fluorinated ethylene propylene (FEP) film (0.1 mm thickness, Dotbit) and exposed for 0.2 s to 365 nm light (Omnicure, AC 475) at 3200 mW cm^{-2} (640 mJ cm^{-2} dose). Droplets were then immediately imaged on an inverted microscope (Olympus IX3 equipped with a 2 × objective) to obtain a pre-swelled image. Droplets were swelled in HBSS for 24 h at room temperature. Swelled droplets were then placed on FEP film and imaged to get a post-swelled image. Droplet diameters were measured from pre- and post- swelling images using ImageJ and averaged for each group to calculate the change in gel volume due to swelling. Three replicate samples were measured for each resin condition.

2.3. 3D printing using BioPµSL

Digital models, including a microgrid, a sphere with a smiley face, microneedles, and a gyroid were designed and converted to STL files using Solidworks. The custom-built digital light processing (DLP) system was used to print various structures as described in previous work [46]. Three-dimensional (3D) printing of resin occurred in a bottom up manner in a vat with FEP film bottom (0.1 mm thickness, 95% light transmission, Dotbit). An image was projected to the bottom of a photopolymerizable resin in a layer by layer fashion (25 µm layer each) using an LED projector with a 405 nm wavelength light source and an intensity of 500 mJ cm^{-2}.

After printing, prints were submerged in the printing resin and dimensions were measured using a confocal microscope (Zeiss LSM 700). Dimensional error between the print and the computer aided design (CAD) was calculated as the absolute difference between CAD dimension and print dimension divided by CAD dimension multiplied by 100, which is shown in the equation below,

$$\text{Dimensional error } (\%) = \frac{|\text{CAD dimension} - \text{Print dimension}|}{\text{CAD dimension}} \times 100.$$

2.4. Fabrication of microgels using BioIDEA

Microgels were produced using a custom built BioIDEA developed based on previous work [23]. A Nordson Ultimus V Pressure Pump nominally set to 35 psi (800 µl min^{-1}, Elveflow MFS3) was used to dispense resin through 100 µm nozzles (Nordson EFD PN: 7018 462). The resulting stable jet was sheared by mechanical oscillation of the nozzle at various frequencies (Mighty Dwarf 7 W Conduction Speaker). This oscillation generated instabilities in the jet, causing discrete droplets to break off. Droplets were then cured in-air between the nozzle and a collection bath using a Phoseon FL400 UV lamp operating at an intensity of 9.42 W cm^{-2} at 365 nm at the droplet stream 5 mm away. We selected 365 nm for our BioIDEA system to ensure fast gelation and prevent coalescence of droplets mid-air as it has been shown that LAP has a peak absorbance at 375 nm [47].

Cured microgel droplets were collected into a continuously stirred bath of HBSS (Gibco 14 025 092). Droplet breakup was visualized and tuned using a high-speed camera (Nova S9 Photron Fastcam) at 40 000 fps.

Droplet size can be controlled by the flow rate of the jet, the size of the nozzle, and the applied frequency of vibration [48–50]. Therefore, a frequency sweep was performed to pinpoint vibration frequencies that consistently generated monodisperse droplets and to explore our ability to tune droplet size. For each frequency, microgels were imaged using an inverted microscope (Olympus IX83) with a 2× objective. Microgel diameters were measured manually using ImageJ ($n > 50$), converted to volumes assuming spherical volume (4/3 *Pi* radius^3), and the cumulative frequency distribution was calculated. Microgel volume is reported since this enabled us to determine coalescence of individual droplets more easily (i.e. 1 vs 2 droplets).

Microgels were fabricated with two concentrations of photoinitiator (0.3% and 0.15%) and various levels of UV intensity (0.47–9.42 W cm^{-2}) to determine the material and fabrication parameters that would lower radical generation during polymerization but prevent coalescence. UV dose was calculated by multiplying UV intensity by exposure time $\left(\tau = l/V_j\right)$ where l is length of the UV lamp and V_j is velocity of the jet. To characterize the degree of coalescence between each condition, microgel diameter and the length of the overlapping region between microgels, or the 'waist', were measured and their ratio was taken. Measurements were taken of microgels ($n > 50$) from three different images per condition.

2.5. Cell culture

4T1 murine mammary gland carcinoma cells (ATCC, CRL-2539) were maintained in RPMI 1640 (ATCC, 30–2001) supplemented with 10% FBS (ThermoFisher A3160502) and 1% penicillin-streptomycin (ThermoFisher15140122) in humidified incubators at 37 °C and 5% CO_2. Cells were passaged every 2–3 d when they reached 90% confluence by briefly rinsing with 0.25% trypsin-EDTA (ThermoFisher 25 200 056), incubating with fresh 0.25% trypsin-EDTA until cells detached, and then resuspending in fresh culture media at a 1:6 or 1:8 split for subculturing. Cells below passage 10 were used for experiments and tested negative for mycoplasma.

2.6. Encapsulation of cells in bulk hydrogels, 3D printed scaffolds, and microgels

4T1 cells were harvested, centrifuged, and resuspended in uncured resins at a density of 3×10^5 cells ml^{-1}. We chose a cell concentration of 3×10^5 cells ml^{-1} as this concentration did not alter droplet breakup for BioIDEA fabrication and we aimed to keep fabrication parameters consistent across experiments. For bulk hydrogel experiments, 200 µl of cell-resin solution was dispensed into the wells of a 48 well plate and cured using a 365 nm lamp with an intensity of 3.3 mW cm^{-2} for 3 min (594 mJ cm^{-2} dose) to simulate 3D printed constructs using the BioPμSL system. The BioIDEA resin was crosslinked using a 365 nm light (Omnicure AC475) with an intensity of 3200 mW cm^{-2} for 0.2 s (640 mJ cm^{-2} dose) to simulate microgel fabrication using BioIDEA. After crosslinking, 300 µl media was added to each well.

Three-dimensional (3D) printing using BioPμSL was performed as previously described in section 2.3. All printing components were autoclaved before use, and the printing was performed in a fully sterilized environment.

For in-air microgel cell encapsulation experiments, the cell-resin solution was passed through a 40 µm cell strainer to prevent cell clumps. Microgel fabrication using BioIDEA was performed as previously described in section 2.4, however all fluidic components were autoclaved for sterility and microgels were collected in a continuously stirred bath of 30 ml sterile cell culture media.

Bulk hydrogels, cell embedded 3D printed structures, and microgels were cultured in cell culture media in a humidified incubator at 37 °C and 5% CO_2. Cell culture media was changed at day 2 for the samples grown for three days.

2.7. Cell viability for cell-embedded bulk hydrogels, 3D printed constructs, and microgels

Viabilities of cells within cell embedded bulk hydrogels, 3D printed structures, and in-air fabricated microgels were evaluated on 1 and 3 d after fabrication. Cell culture media was removed, and samples were rinsed with PBS twice. Live-dead staining solution was made by adding 1 µl ml^{-1} calcein AM and 2 µl ml^{-1} ethidium homodimer-1 (ThermoFisher L3224) in PBS. Samples were incubated in the staining solution for 30 min at room temperature, then rinsed with PBS twice, put in HBSS and imaged with a confocal microscope (Zeiss LSM 700). For bulk hydrogels, 500 µm z-stacks were taken (step size: 3.2 µm) for three different regions within each well, and three wells were imaged per condition using a 10× objective. Maximum intensity projections were used to quantify viability. For BioPμSL prints, five images were taken throughout the printed microgrid scaffold using a 10× objective for three constructs ($n = 3$). BioIDEA fabricated microgels were dispensed in a glass bottom dish ($n = 2$) and 10 images were taken of different regions using a 2.5× objective to visualize multiple microgels in one image. The number of live and dead cells for each sample was quantified using an open-source macro in ImageJ [51]. The default thresholding method and limits

were adjusted to ensure accurate processing of our images and were kept constant between conditions. Viability was calculated as the percentage of live cells over the total cell count.

2.8. Microgel stacking

Microgels were fabricated using three PEG-thiol-ene resins with different storage moduli (10 wt% PEG-SH 3.5k–0.5 kPa, 7.5 wt% PEG-SH 3.5k–3.7 kPa, and 4.3 wt% PEG-SH 3.5k–13.9 kPa). For better visualization, 1 mg ml^{-1} of different fluorophore molecules were added to each resin to demonstrate the ability to stack microgels into a porous gradient tissue scaffold in a controlled layer-by-layer approach. The extrusion pressure was adjusted as necessary for each to produce a stable jet (10 wt% PEG-SH + 20k FITC Dextran—40 psi, 7.5 wt% PEG-SH + 10k Cascade Blue—40 psi, and 4.3 wt % PEG-SH + 20k TRITC Dextran—35 psi). Microgels were strained from their HBSS catch solution using a 300 μm cell strainer and placed in a 50 ml conical tube. The 1 mg ml^{-1} fluorophore solution was added to each tube to resuspend the microgels to roughly 25% v/v for storage. Gradient stiffness scaffolds were constructed with the microgels by dispensing 500 μl of microgel solution onto the apical chamber of an 8 μm polycarbonate membrane Transwells (Greiner Bio 665110) and centrifuging for 1 min at 150 rcf (Eppendorf 5804 R, A-2-DWP rotor) with acceleration (0.852 rcf s^{-1}) and deceleration (0.794 rcf s^{-1}) at levels = 1. These steps were repeated with each microgel solution to create the desired layer order. Microgels were washed 3× by pipetting 500 μl HBSS on top of the scaffold and centrifuging to wash away any fluorescent solution from the scaffold pores. Scaffolds were crosslinked by pipetting 200 μl of a 2% PEG-NB (20k) and 0.3% LAP solution to the scaffold, centrifuging and exposing the scaffold to a 32 μW cm^{-2} 365 nm light source for 3 min. Crosslinked porous gradient scaffolds were removed from the Transwell by cutting out the circular bottom membrane with a scalpel and imaged using a Zeiss LSM 980 with a 2× objective.

2.9. Statistical analysis

Linear and nonlinear regression were used to test if storage modulus, expansion ratio, and gelation time correlated with PEG-SH and photoinitiator concentration (figures 2(a) and (b)). Two-way ANOVA was performed to determine differences in storage modulus, expansion ratio, and crossover time across gel formulations (figure 2(c)). Two-sample Kolmogorov–Smirnov tests were used to determine differences between microgel population size distributions (figure 5(b)). Differences in microgel waist-to-diameter ratio (figure 5(d)) and viability data (figures 6(b) and (d)) were determined using a two-way ANOVA with Tukey post hoc comparisons. All data are presented as means ± standard deviations. Significance was defined as $p < 0.05$ for all statistical tests.

3. Results

3.1. Rheological and swelling characterization of PEG-thiol-ene hydrogels

PEG-thiol-ene prepolymer resins with excess thiol groups were prepared and tested with shear oscillatory rheology under illumination for 3 min to determine the effects of varying the PEG-SH molecular weight and concentration as well as photoinitiator concentration on modulus, swelling, and gelation time of our thiol-ene hydrogels (figure 1).

Increasing PEG-SH from 5 wt% (SH:NB = 1.4) to 10 wt% (SH:NB = 2.0) decreased the storage modulus from 5.6 ± 0.1 kPa to 0.65 ± 0.03 kPa (with a statistically significant linear regression coefficient −1014 Pa/wt% PEG-SH, $p < 1 \times 10^{-4}$, figure 2(a)). This result is in accordance with previous studies that stoichiometrically balanced thiol-norbornene materials (SH:NB closer to 1) showed higher modulus than thiol-norbornene materials with lower stoichiometric ratios [52, 53]. Correspondingly, the expansion ratio increased from 2.9 ± 0.1 to 5.7 ± 0.6 (regression coefficient of 0.59, $p < 1 \times 10^{-4}$). In contrast, the gelation time remained similar (0.45 s) and non-significant ($p = 0.1482$) for all PEG-SH concentrations.

Next, LAP concentration was varied from 0.01 to 0.6 wt% while PEG-NB (5 wt%, 20 kDa) and PEG-SH (5 wt%, 3.5 kDa) concentrations were kept constant. The storage modulus ($p = 0.75$) and expansion ratio ($p = 0.17$) remained similar for all conditions (figure 2(b)). As expected, the gelation time decreased exponentially as LAP concentration increased, from 2.2 s to 0.4 s with little change in gelation time from 0.3% (0.46 ± 0.03 s) to 0.6% (0.4 s).

Lastly, the concentration and molecular weight of PEG-SH was varied while concentration of PEG-NB and LAP were kept constant (figures 2(b) and (c)). Changing the molecular weight of the PEG-SH from 3.5 kDa to 5 kDa resulted in an increase of final storage modulus from 5.6 ± 0.1 kPa to 11.5 ± 0.01 kPa for 5 wt% PEG-SH and 0.5 ± 0.01 kPa to 4.5 ± 0.1 kPa for 10 wt% PEG-SH. The expansion ratio of 3.5 kDa and 5 kDa for 5 wt% PEG-SH were not significant. Gelation times were similar across all conditions and not significant.

The rheological properties for BioPμSL resin were measured to have storage modulus of 2.47 ± 0.30 kPa, expansion ratio of 4.9 ± 0.3, and gelation time of 61.0 ± 1.6 s (Table 1). BioPμSL resin showed slow gelation time due to the addition of the photoabsorber, QY, in the resin. For BioIDEA resin, we selected 5 wt% PEG-SH (3.5k) and 5 wt% PEG-NB (20k) as the precursors with 0.3 wt% photoinitiator since this formulation provided a modulus similar to mammary gland tumors [54] while retaining a gelation

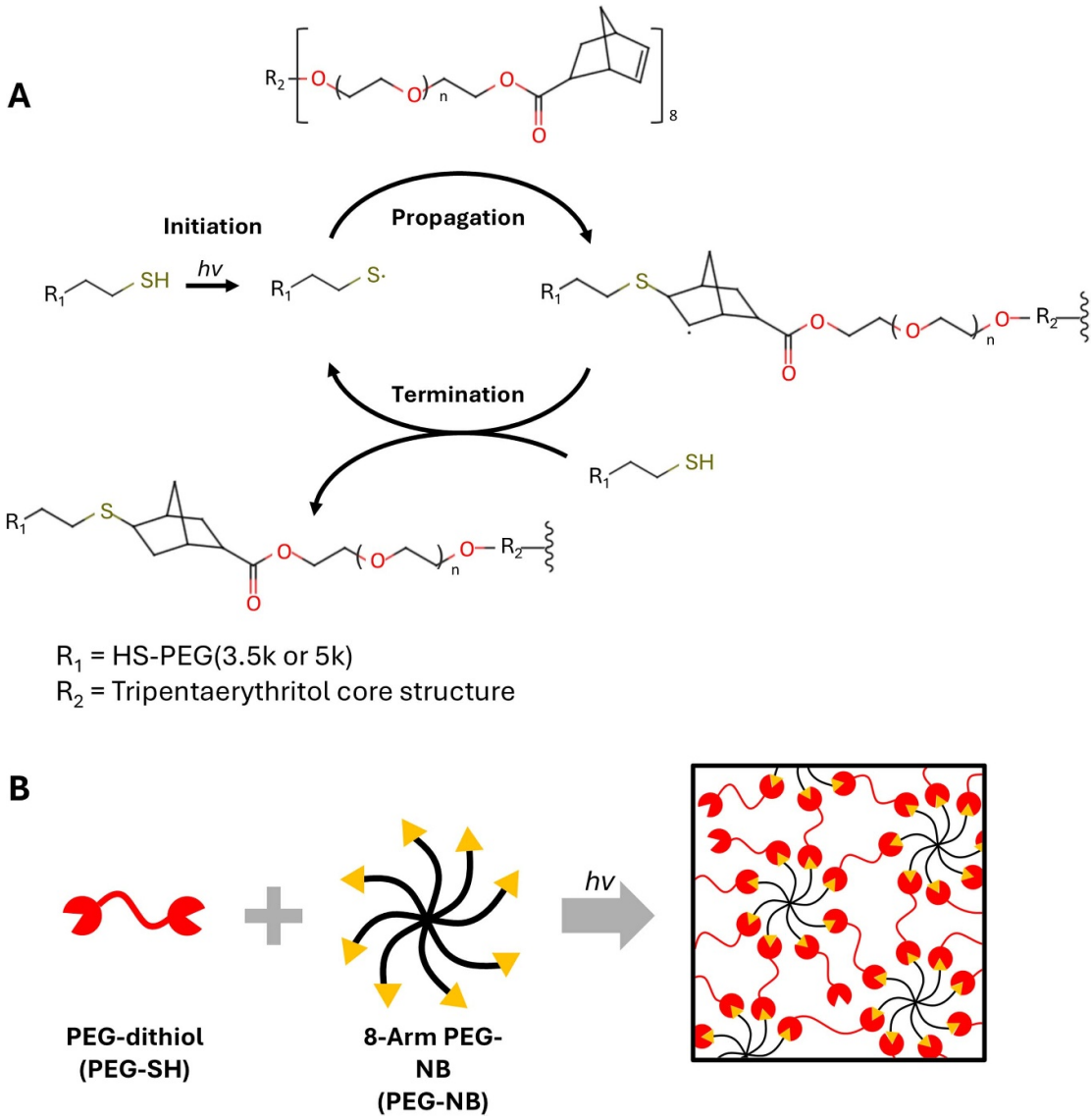

Figure 1. (A) A schematic of thiol-norbornene photoclick reaction showing radical mediated step growth. (*hv*: light irradiation). (B) An illustration of PEG-thiol-ene network formation using photoclick reaction between PEG-dithiol and 8-arm PEG-NB. An excess of thiol groups can be used to crosslink microgels together or modify the material.

time < 0.5 s, key to achieving reproducible in-air microgel formation.

3.2. 3D printing using BioPμSL

To demonstrate the printability of PEG-thiol-ene bioresins, various structures were printed using our DLP 3D bioprinter, BioPμSL [46], using a bottom-up printing setup (figure 3(a)). While the BioPμSL is capable of switching back-and forth between bottom-up and top-down printing setups, we chose the bottom-up printing setup as it consumes less resin and increases the leveling rate of resins compared to top-down printing [55], which decreases the overall build time. The short printing time can be particularly beneficial if the printing resin contains live cells since decreasing the time in which cells spend in the bioresin can increase the cell viability [56]. We selected 10 wt% PEG-SH (5k) and 5 wt% PEG-NB (20k) as the precursors of the BioPμSL resin. The concentrations of the photoinitiator (LAP) and the photoabsorber (QY) were optimized using microgrid CAD design to achieve a dimensional error between the CAD design and actual print less than 5%.

After optimizing the resin composition and 3D printing parameters such as layer thickness and dosage, we demonstrated that we could generate multiple complex 3D structures including a microgrid, a sphere with smiling face, microneedles, and a gyroid, using the BioPμSL resin. Figure 4 shows the top and side views of CAD images and their corresponding printed structures after swelling in PBS to equilibrium at the bottom. All prints showed isotropic, reproducible swelling, (supplementary figure 1) thus to

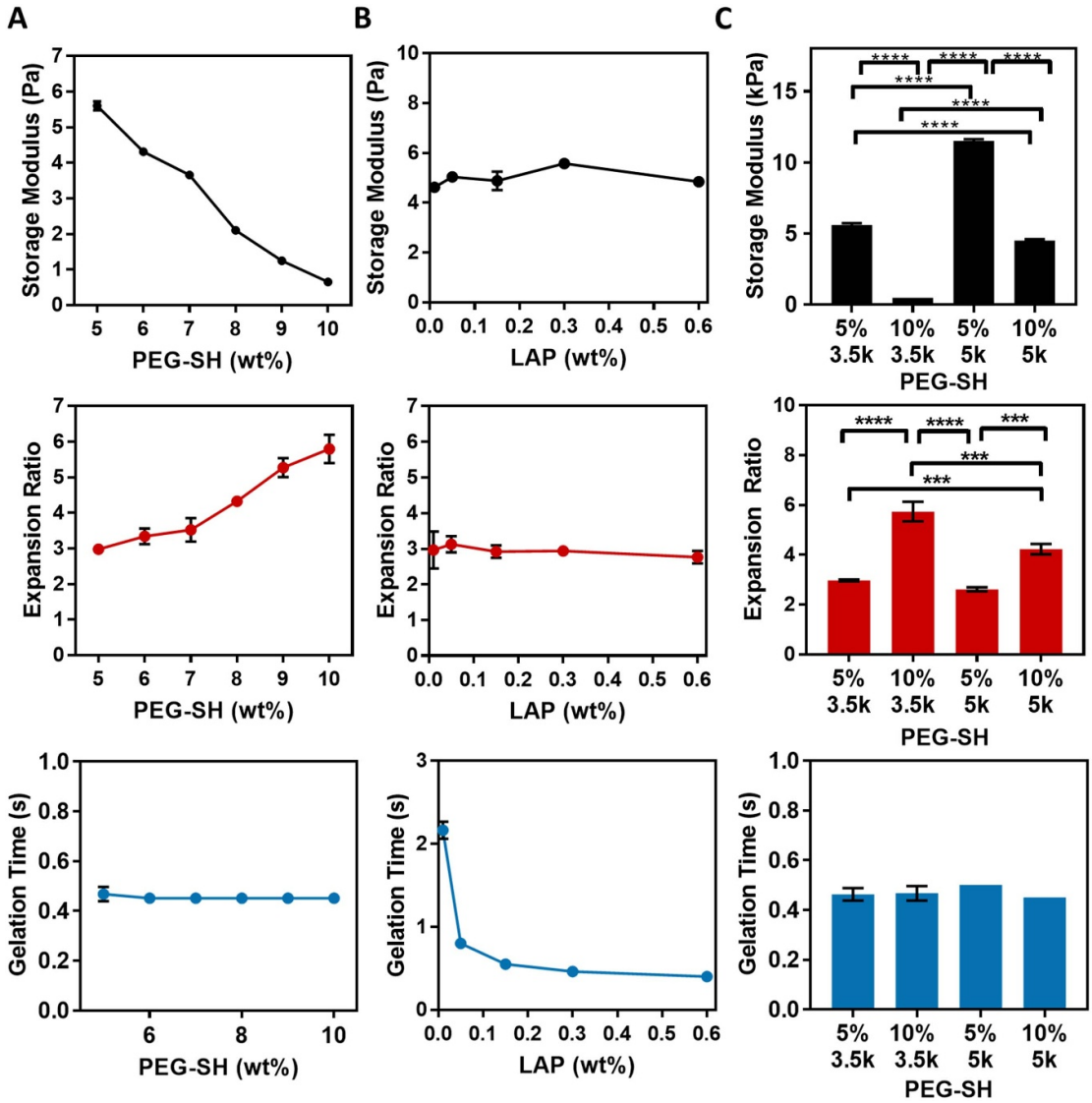

Figure 2. Rheological properties of PEG-thiol-ene hydrogels. (A) Storage modulus, expansion ratio and gelation time of PEG-thiol-ene hydrogels made with varying concentrations of PEG-SH (3.5k), 5 wt% PEG-NB (20k) and 0.3 wt% LAP. (B) Storage modulus, expansion ratio and gelation time of PEG-thiol-ene hydrogels made with varying concentrations of LAP, 5 wt% PEG-SH (3.5k) and 5 wt% PEG-NB (20k). (C) Storage modulus, expansion ratio and gelation time of PEG-thiol-ene hydrogels made with 5 wt% PEG-NB (20k), 0.3 wt% LAP and PEG-SH with two different molecular weights of 3.5k and 5k. ***,**** represent $p < 0.001$ and $p < 0.0001$, respectively. Bar graphs with no error bars indicate a standard deviation of zero.

Table 1. Rheological and swelling data for PEG thiol-ene resins used for 3D bioprinting and in-air photopolymerization.

	BioPμSL resin	BioIDEA resin
Formulation	10% 5 kDa PEG-SH, 5% 20 kDa PEG-NB, 0.01% LAP, 0.04% QY	5% 3.5 kDa PEG-SH, 5% 20 kDa PEG-NB, 0.3% LAP
Storage modulus (kPa)	2.47 ± 0.30	5.61 ± 0.12
Expansion ratio	4.9 ± 0.3	2.98 ± 0.04
Gelation time (s)	61.0 ± 1.6	0.46 ± 0.03

obtain a final structure with desired dimensions we chose to undersize the printed dimensions [57].

The microgrid prints showed homogeneously and isotropically swollen dimensions of the strut across the structure. The smiley face print showed clear negative spacing on its eyes and mouth, where the CAD dimensions for the eye diameter and the smallest width of mouth were 200 µm and 100 µm respectively. The microneedle print showed that small square pyramids with a base side length of 500 µm and a height of 1 mm can be printed. We also demonstrated that complex and porous gyroid scaffolds that cannot be produced with molding [58] can be printed with the BioPμSL resin, which can be beneficial for use as

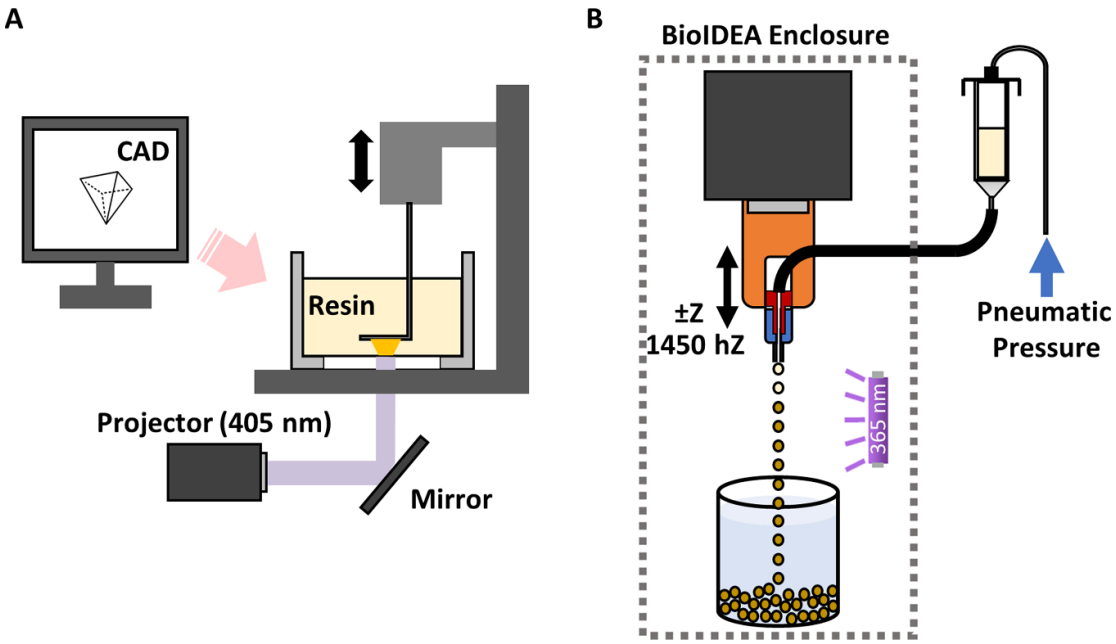

Figure 3. Schematics of microgel fabrication and 3D printing techniques. (A) BioPμSL bottom-up printing system with 405 nm light source. (B) Biological In-Air Drop Encapsulation Apparatus (BioIDEA).

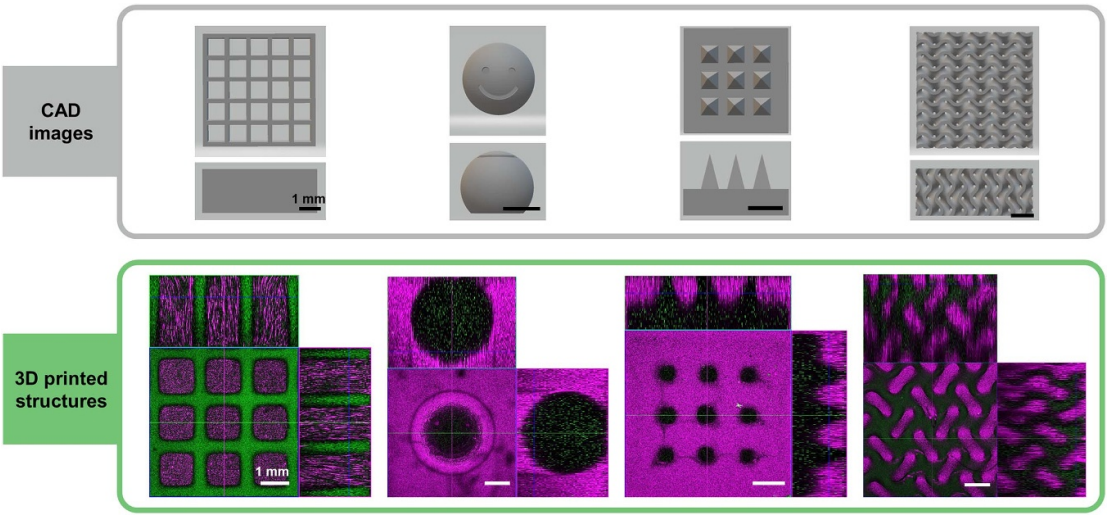

Figure 4. Various 3D printed structures using PEG-thiol-ene resin. Top: top and side views of computer aided designs (CADs) that were used to print each structure (left to right: microgrid, sphere with smiley face, microneedles, gyroid). Scale bar: 1 mm. Bottom: confocal images of each structure post-swelling showing the top view and perpendicular cross section views. All prints (green) were submerged in PBS containing 1 μm red fluorescent beads (shown as magenta). Scale bars: 1 mm.

cell-laden tissue scaffolds. The gyroid geometry has been widely used as tissue scaffolds due to its robustness and high porosity which allows sufficient nutrient and waste diffusion [58, 59]. Overall, our results indicated that multiple small and complex morphologies can be printed using the same BioPμSL resin and the printing parameters.

3.3. Microgel fabrication using BioIDEA

Microgels were produced using BioIDEA (figure 3(b), supplementary figure 2). The vibration frequency was varied to examine its effect on microgel size and pinpoint frequencies that resulted in repeatable microdroplet breakup and monodispersity. High-speed video captured the microdroplet formation from the nozzle to the UV curing zone (supplementary figures 3–5). Analysis of high-speed videos indicated that for applied frequencies of 2175 Hz and 4360 Hz, coalescence occurred near the nozzle resulting in lower measured frequencies 1143 Hz and 1504 Hz, respectively, of droplets passing through the UV curing zone (supplementary figures 3–5). Therefore, the measured droplet production frequency was used to plot microgel volume

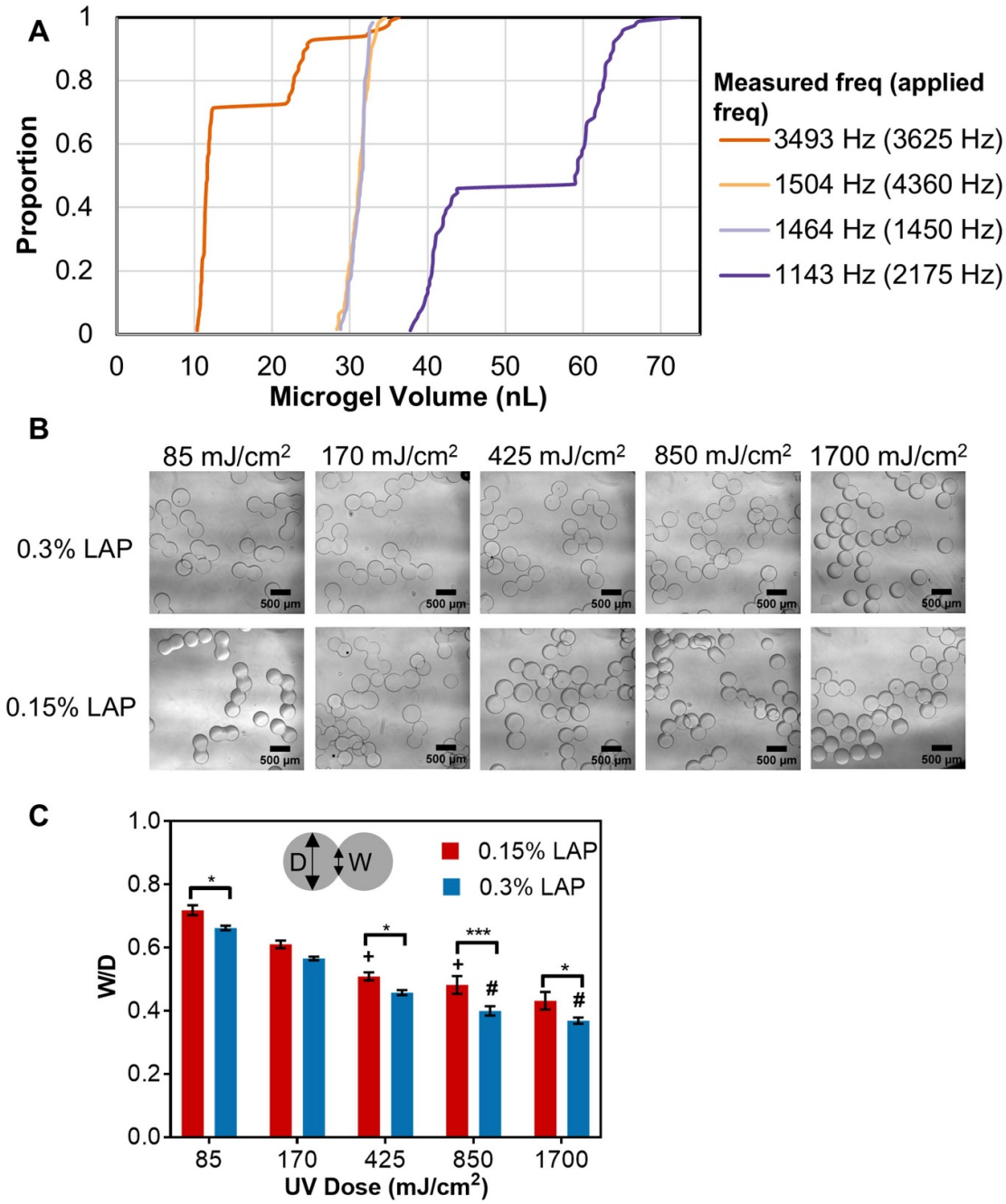

Figure 5. In-air microgel fabrication and characterization. (A) Microgel volume as a function of measured droplet production frequency. Applied frequencies are noted in parentheses. (B) Microgels fabricated with varying levels of photoinitiator (LAP) and UV dose. Scale bars: 500 µm (C) Microgel waist-to-diameter (W/D) ratio indicates decreasing degree of coalescence for higher levels of LAP and UV dose. *,**, *** indicate $p < 0.05$, 0.01, and 0.001, respectively. Bars plots with like symbols indicate conditions that are not significant from one another. All other UV dose conditions within the same LAP concentration are significant ($p < 0.05$).

distributions. This observed coalescence is verified by the two microgel volume populations for these frequencies (figure 5(a)). For 3943 Hz, the majority of microgels are 11 nl in volume whereas a smaller proportion are 22 nl in volume indicating coalescence of two droplets occurred at some point mid-air. For 1143 Hz, nearly half of the microgels are ∼41 nl in volume and the other half are ∼63 nl in volume, again indicating coalescence of droplets mid-air. For an applied frequency of 4360 Hz, coalescence occurs near the nozzle and resulted in monodisperse droplets entering the curing zone at a measured frequency of 1504 Hz and therefore we obtained more uniform cured microgels with a diameter of 398 ± 38 µm (supplementary figure 6). Alternatively, for an applied frequency of 1450 Hz there was no observed coalescence in the high-speed videos resulting in a similar measured droplet production frequency of 1464 Hz. As a result, there is only one population of microgel volume for this

frequency indicating less mid-air coalescence and more monodisperse cured microgels with a mean diameter of 398 ± 4.4 μm (**s**upplementary figure 6). Therefore 1450 Hz was chosen for all subsequent experiments. Importantly, microgel volume and diameter decreased as measured droplet production frequency increased (figure 5(a), supplementary figure 6) indicating that this parameter can be tuned to control microgel size. Microgels fabricated with PEGDA resin resulted in a higher degree of coalescence and therefore larger microgels than the thiol-ene resin (supplementary figure 7) due to curing kinetics that were 3.8× slower (1.76 ± 0.1 s) than the thiol-ene resin (0.46 ± 0.03 s).

We next explored microgel fabrication using different levels of photoinitiator concentration and UV intensity. We chose 0.15% and 0.3% photoinitiator because the rheology data showed that gelation time plateaued at 0.46 ± 0.03 s for 0.3% and increased to >0.8 s for concentrations below 0.15% which would have led to increased coalescence of microgels. Microscopy images of microgels fabricated with 0.15% and 0.3% photoinitiator showed decreasing coalescence of microgels as UV dosage increased from 85 mJ cm^{-2} to 1700 mJ cm^{-2} (figure 5(b)). This visual decrease in coalescence is supported by the decreasing ratio between the length of the overlapping region between microgels, or the 'waist', to microgel diameter (W/D) which decreased from 0.72 ± 0.02 at 85 mJ cm^{-2} to 0.43 ± 0.03 at 1700 mJ cm^{-2} for 0.15% LAP indicating a lower degree of overlap between joined microgels (figure 5(c)). UV doses above 425 mJ cm^{-2} gave a waist-to-diameter ratio ⩽ 0.5 for both 0.15% and 0.3% photoinitiator resulting in more distinct and well-formed microgels. As a result, 425 mJ cm^{-2} and 1700 mJ cm^{-2} were selected to study cell viability after encapsulation to determine how UV dose and photoinitiator concentration affect viability.

3.4. Cell viability of 3D printed microgrids and in-air photopolymerized microgels

Having demonstrated that PEG-thiol-ene resins can be readily tuned to achieve various mechanical stiffness and that such resins can be used to create microporous scaffolds with BioPμSL and BioIDEA technology, we wanted to demonstrate the potential application of the microporous PEG-thiol-ene scaffolds in heterogeneous tissues such as tumors that are known to have heterogeneity in stiffness, cell population, and gene expression [54, 60–62]. We chose mouse the mammary gland cancer cell line, 4T1 cells, to evaluate the cell viability in the PEG-thiol-ene resins and their potential for use in heterogeneous tissue fabrication for diagnostic or therapeutic applications. The cell viability in the bulk gels made with BioPμSL resin and in the 3D printed microgrid structures were demonstrated by performing a live/dead assay on 1 and 3 d after culture (figures 6(a) and (b), supplementary figure 8). Figures 6(a) and (b) shows that the cell viabilities in the BioPμSL bulk gels and 3D printed microgrids were similar and not significantly different (>70% for Day 1, >65% for Day 3). This indicates that 3D printing process where cells need to be in the uncured resin for 30 min to 2 h do not decrease the cell viability in the printed structures significantly.

To understand how fabrication parameters like UV intensity and photoinitiator concentration influence acute cell viability after encapsulation using BioIDEA and BioIDEA resins, 4T1 cell-laden microgels were fabricated using varying LAP concentrations and UV intensities. Bulk gels were prepared to serve as a control using a similar photoinitiator concentration (0.3 wt%) and UV dose (640 mJ cm^{-2}) as the microgels fabricated using BioIDEA. After culturing the cell-laden structures for 1 d, 4T1 cells in microgels fabricated with 425 mJ cm^{-2} had a significantly higher viability than those fabricated with 1700 mJ cm^{-2} for both 0.15% (85 ± 5%, 64 ± 18%, $p < 0.00)1$ and 0.3% photoinitiator (85 ± 7%, 58 ± 21%, $p < 0.0001$) (figures 6(c) and (d)). The means of the microgel samples were not significantly different than the bulk gel. On day 3, the differences in cell viability became more distinct and all conditions were significantly lower from their day 1 counterparts. Despite experiencing similar UV dose and photoinitiator concentration, microgels fabricated with 425 mJ cm^{-2} showed significantly higher cell viability (0.15%–52 ± 11%, 0.3%–48 ± 13%) than the bulk gels (0.3%–26 ± 10%). These results show that using lower UV dosage during BioIDEA fabrication leads to higher cell viability in the cell-laden microgels. While not significant, microgel viability for 1700 mJ cm^{-2} and 0.3% photoinitiator had a higher mean viability (38 ± 13%) than bulk gels (26 ± 10%) despite experiencing an order of magnitude higher UV dose.

3.5. Stacking microgels to form multi-layered tissue scaffolds

To demonstrate the utility and versatility of using BioIDEA fabricated microgels to generate heterogenous tissue scaffolds, microgels were stacked in a layer-by-layer fashion and underwent a secondary crosslinking to form a tissue scaffold with a gradient in stiffness. Crosslinked scaffolds were able to be handled and stood unsupported once removed from the Transwell. Figure 7(a) shows a macroscopic view of the resulting gradient scaffold with stiff microgels (13.9 kPa) on the bottom in magenta and soft microgels (0.5 kPa) on top in green. Figure 7(b) shows a microscopic cross-sectional view of the gradient construct showing three distinct layers of microgels with different stiffness. While the stacked construct does not contain cells embedded within the microgels, the scaffolds demonstrated the ability to spatially control deposition of microgels with various stiffnesses and properties to produce a porous gradient scaffold.

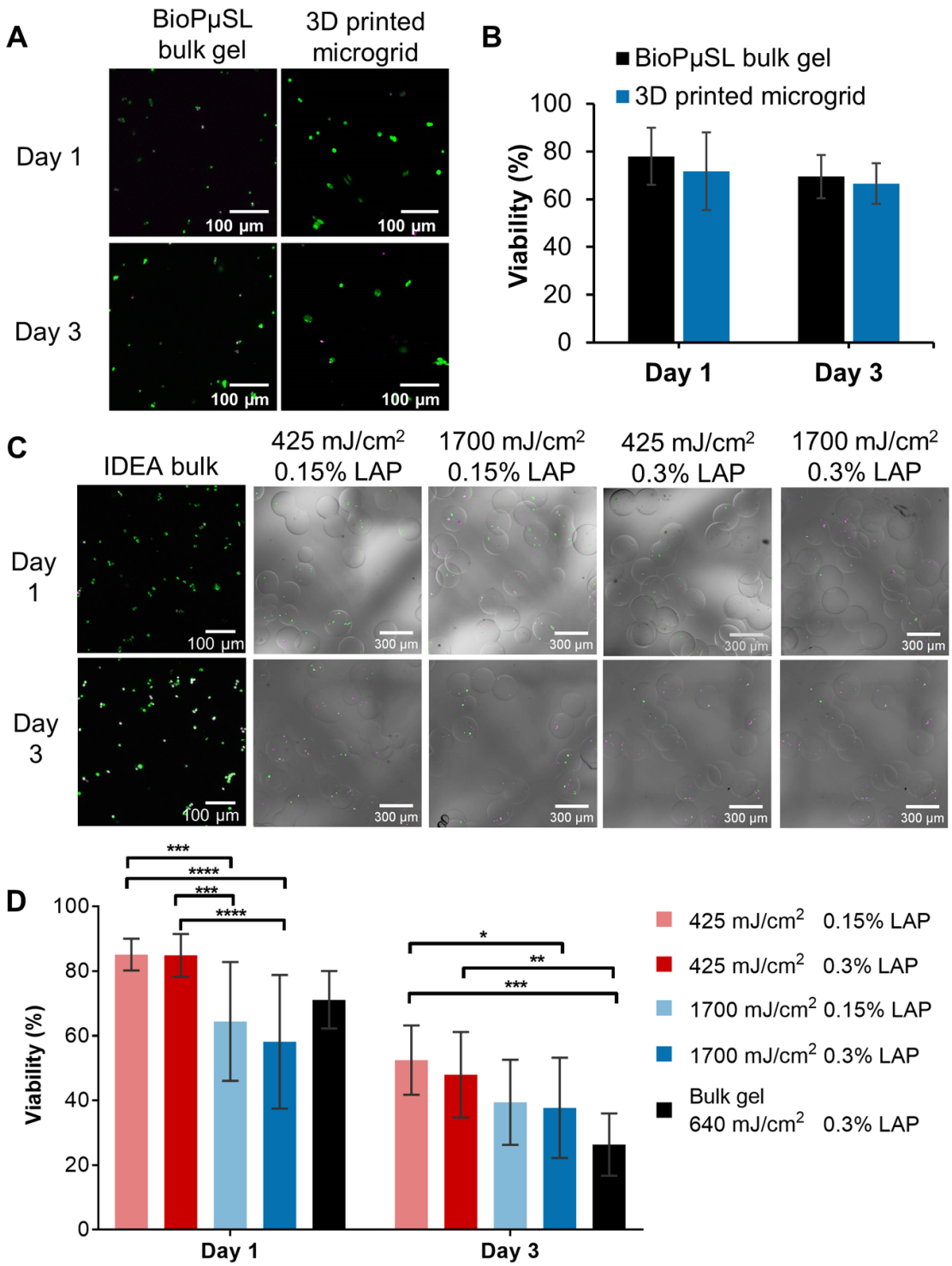

Figure 6. 4T1 cell encapsulation in PEG-thiol-ene hydrogels fabricated using BioPμSL and BioIDEA. (A) Live/dead images of 4T1 cells cultured in BioPμSL bulk gels and printed microgrids on day 1 and 3 (green: live cells, magenta: dead cells). (B) Viability of 4T1 cells in BioPμSL bulk gels and printed microgrids on day 1 and 3. (C) Live/dead images of 4T1 cells cultured in BioIDEA bulk gels and microgels fabricated with varying photoinitiator (LAP) concentration and UV power on day 1 and 3 (green: live cells, magenta: dead cells). (D) Viability of 4T1 cells in the BioIDEA resin bulk gel and microgels on day 1 and 3. *, **, ***, **** indicate $p < 0.05$, 0.01, 0.001, and 0.0001, respectively. All conditions on day 3 were significant from their counterpart on day 1.

4. Discussion

The goal of this study was to utilize the known versatility of PEG thiol-ene resins to enable production of heterogeneous, complex cell-laden tissue scaffolds for tissue engineering applications. Fabrication techniques such as 3D bioprinting or in-air photopolymerization of microgels are complimentary techniques, which can either be used independently or in combination, to enable the reproduction of spatial organization of tissues. Therefore, we aimed to develop versatile PEG thiol-ene formulations

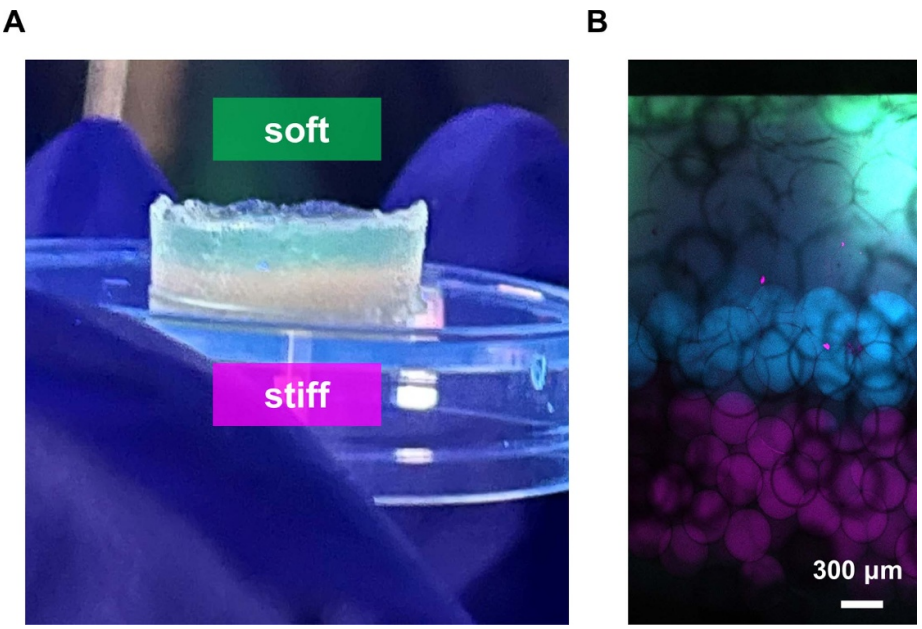

Figure 7. (A) BioIDEA fabricated microgels with excess thiol groups were stacked and underwent a secondary crosslinking to form a tissue scaffold with a gradient in stiffness. (B) Microscale image of a cross-section of the crosslinked scaffold showing three distinct layers of stiffness (magenta—13.9 kPa, blue—3.7 kPa, green—0.5 kPa).

suitable for multiple fabrication modalities. Here, we developed photopolymerizable formulations with varying stiffness and identical crosslinking conditions that can be used for fabrication of both cell-laden 3D bioprinted structures and in-air fabricated microgels.

We chose PEG-thiol-ene resin for fabrication of cell-laden tissue scaffolds due to the facile thiol-ene reaction chemistry [38], rapid curing, biocompatibility [30, 63, 64], and tunable chemistry which directly influences mechanical properties of PEG polymers [65]. Using this material, mechanical properties such as storage moduli and swelling ratios could be controlled independently from gelation time by modulating the thiol to norbornene ratio or the molecular weights of PEG-SH in the resin. Storage moduli of the PEG-thiol-ene hydrogels ranged from 0.5 kPa to 12 kPa, which is in the range of mechanical moduli for various soft tissues in humans (brain, 0.1–1 kPa; adipose tissue, liver, 1–10 kPa; muscle, 8–15 kPa) [66, 67]. The controllable swelling properties of the PEG-thiol-ene hydrogels may be beneficial as a drug delivery platform since the drug loading and release kinetics could be controlled using the variation in the swelling properties [68, 69].

The quick and consistent gelation time of the PEG-thiol-ene resins across multiple formulations is very advantageous for both DLP bioprinting and the in-air photopolymerization technique. For DLP bioprinting, this unique feature of PEG-thiol-ene resin may enable fabrication of multi-material tissue structures using various formulations without changing printing parameters such as exposure time, layer thickness, or light intensity. For the in-air photopolymerization technique, it reduces mid-air coalescence and enables the generation of microgels with varying mechanical properties without the need to modify the fabrication parameters such as the applied vibration frequency or UV power for each resin.

The fast gelation kinetics of the PEG-thiol-ene resin enabled low levels of photoinitiator (0.01%) to be sufficient for photopolymerizing each bioprinted layer (25 μm). The higher viability of cells embedded in BioPμSL bulk gels compared to BioIDEA bulk gels (0.3%) could be mainly due to the one order of magnitude lower concentration of LAP in the BioPμSL bulk gels (0.01%) as lower concentrations of photoinitiator have been shown to reduce free radical damage to cell membranes, nucleic acids, and proteins [70, 71]. Additionally, the BioPμSL resin had a higher expansion ratio than the BioIDEA resin which may indicate a higher degree of porosity and therefore better transport. The viability of cells embedded in the 3D printed microgrids did not decrease significantly during three days of culture. This is noteworthy because cells were in the uncrosslinked BioPμSL resin for 30–120 min before three prints could be printed. Cell viability has been shown to decrease significantly with increasing photoinitiator concentration and time spent in the uncrosslinked resin [72]. Our results show that our PEG-thiol-ene resin enabled low levels of photoinitiator and short printing time (30 min/print) which are advantageous features for bioprinting cell-laden tissue matrices. However, the cell-embedded BioPμSL resin showed limited printability when the target

thickness is higher than 150 μm, which could be due to due to the light scattering effect of the embedded cells. Therefore, for future studies, we aim to decrease photoabsorber concentration or increase light dosage to improve the printability for the cell-embedded resins.

The PEG-thiol-ene resin also has high flowability at room temperature therefore increasing printing speed and reducing bubbles generated during printing compared to higher viscosity resins [73]. Resins with high viscosity or thermoreversible gelation may also require heating to increase the flowability of the resin during printing which can lead to evaporation and change in resin properties over time preventing reuse. In contrast, PEG-thiol-ene resins can be reused multiple times, significantly decreasing the amount of resin needed for multiple prints.

The rapid curing of our PEG-thiol-ene resin was key to achieving controllable fabrication of in-air photopolymerized cell-laden microgels via BioIDEA. The thiol-ene resin mitigated mid-air coalescence without needing high concentrations of polymer or photoinitiator that are required for in-air gelation of other biomaterials such as PEGDA [28] which can lead to cytotoxicity [74]. The flowrates used in this study (800 μl min^{-1}) are up to two orders of magnitude higher than droplet microfluidics (1–10 μl min^{-1}) and do not require the use of immiscible oil eliminating two critical bottlenecks in microgel fabrication.

An interesting finding was that the frequency applied to the nozzle to generate breakup of the microdroplets did not always match the measured droplet frequency near the curing region. This coalescence of droplets close to the nozzle may be caused by instabilities in the flow of our material due to heat generation and convective air currents generated during curing. BioIDEA generated microgels of varying size, however some microgels appear to be stuck together in a chaining effect. Future experiments will aim to reduce this effect using surfactants or other methods that prevent interaction of the microdroplets in the air before curing [75]. The presence of cells in the bioresin may also affect droplet breakup and resulting microgel size [75]. Future studies will need to be conducted to test a range of cell concentrations to determine how this parameter effects droplet breakup as well as encapsulation efficiency (the number of cells within each microgel) as this is a stochastic process.

To the best of our knowledge, fabricating cell-laden microgels using the in-air photopolymerization technique has not been demonstrated to date. While other in-air systems have demonstrated cell encapsulation, they rely on enzymatic or ionic crosslinking of microgels, therefore limiting the types of materials that can be used [76–78]. Using photopolymerizable materials offers more flexibility in material choice.

Here we have demonstrated cell encapsulation using in-air photopolymerized microgels for the first time. The mean viability of the embedded cells in microgels was higher compared to bulk gels on day 3, which suggests that microgels likely allow greater diffusion of nutrients and oxygen to the cells than the bulk gels because of their higher surface area to volume ratio. However, the cell viabilities for all conditions decreased from day 1 to day 3 and microgels fabricated with 1700 mJ cm^{-2} were not statistically significant from bulk gels. This decrease in viability is most likely due to free radicals generated during photopolymerization and the use of UV light to achieve fast gelation. Radical damage may be reduced by incorporating radical scavengers in the resin, or by using visible light (405 nm) to polymerize microgels, another key feature, along with lower photoinitiator concentration, of the BioPμSL resin which may have led to higher viability. Future studies will explore how to achieve fast gelation for uniform microgel fabrication while maintaining high cell viability.

In addition, the combined effect of shear stress generated from nozzles and the time cells spent in the uncured resin can play a role in lowering cell viability relative to controls [79]. Cells also incidentally spent more time in the uncured resin for the 1700 mJ cm^{-2} condition which may have contributed to the lower viability than the 425 mJ cm^{-2} condition. Future experiments will need to pinpoint the short- and long-term effects these phenomena have on cell viability and function as well as test additional cell types.

Finally, the properties of the material itself may influence cell viability. While the PEG thiol-ene resin enabled controllable and reproducible fabrication of cell laden microgels using the BioIDEA technique, future studies must focus on improving the biocompatibility of the material. The PEG thiol-ene resin is versatile and may be modified to include cell adhesive peptides as well as protease degradable crosslinkers to enable cells to adhere, degrade, and remodel the material over time which may enhance cell viability [11]. Improving cell adhesive and degradable properties of the PEG thiol-ene material will allow us to utilize other anchorage dependent cell types to analyze cellular interaction with the material and evaluate the biocompatibility of the material. Additionally, other thiol-ene modified natural materials such as gelatin and hyaluronic acid may be explored as these have shown to be highly biocompatible [80, 81].

While stereolithographic bioprinting excels at fabricating ordered, microscale living structures, it currently has limited options to produce structures possessing a gradient of stiffness and compositions. We developed a layer-by-layer method to stack and crosslink our BioIDEA fabricated microgels into a gradient stiffness construct using only a centrifuge and handheld UV lamp. These are tools that can be

found in virtually any lab therefore eliminating the need for specialized equipment to generate gradient tissue constructs. While we have demonstrated that we can tune our resin to have excess thiol groups that can be utilized for secondary crosslinking of microgels, these excess thiol groups may also be used to functionalize the material to contain spatiotemporal biochemical cues or protease degradable crosslinks, highlighting the versatility of the thiol-ene resin for BioIDEA fabricated microgels. Additionally, scaffold porosity can be tuned independent of microgel mechanical properties simply by changing microgel size or stacking parameters providing a clear benefit over bulk hydrogels. The high-throughput fabrication of cell-laden microgels via BioIDEA enables the scalable construction of modular, microporous complex tissue scaffolds not achievable with current fabrication methods.

While our proof-of-concept scaffold does not yet contain cells, future work will focus on characterizing the number of cells encapsulated within each microgel to enable constructing gradients in cell density, which is important for mimicking gradient tissues. Embedding cells within the microgels, may offer better protection from the host immune system [82], provide custom microenvironments for each cell type [83], and enable control of cell placement within a tissue scaffold. This cell encapsulation technique may be translated to other mammalian cell types as well as bacterial, plant, or algal cells, enabling other technologies such as high-throughput screening of cells for directed evolution, biofuel [84] and biotherapeutic production [85], biosensing, and bioremediation [86].

5. Conclusion

In summary, we have utilized the versatility of PEG-thiol-ene resins to produce cell-laden microporous tissue scaffolds through 3D DLP bioprinting and the in-air photopolymerization technique. Various complex structures could be printed with PEG-thiol-ene resin using the BioPμSL system. In addition, we demonstrated high-throughput fabrication of cell-laden microgels using the BioIDEA. Microgels with varying mechanical stiffness and fast curing time were rapidly produced using BioIDEA and used to generate a gradient tissue scaffold. We anticipate that our PEG-thiol-ene resin along with BioPμSL and BioIDEA technology will allow fabrication of complex and heterogeneous tissues that mimic native tissues and could be utilized in applications beyond tissue engineering such as biosensing and biotherapeutic production.

Data availability statement

The data cannot be made publicly available upon publication because no suitable repository exists for hosting data in this field of study. The data that support the findings of this study are available upon reasonable request from the authors.

Acknowledgment

This work was performed under the auspices of the US Department of Energy by Lawrence Livermore National Laboratory under Contract DE-AC52-07NA27344. The research was supported by LLNL LDRD-22-LW-081. Information release number LLNL-JRNL-861494. This work has been cleared for public release by Los Alamos National Laboratory (LA-UR-24–25864).

ORCID iDs

Lindy K Jang https://orcid.org/0000-0001-6256-1231
Jesse T Ahlquist https://orcid.org/0000-0002-7837-3857
Michael Triplett https://orcid.org/0000-0002-8561-3206
Monica L Moya https://orcid.org/0000-0002-6714-1700
Claire Robertson https://orcid.org/0000-0002-3059-5135
William Hynes https://orcid.org/0000-0003-3628-9486
Elisa M Wasson https://orcid.org/0000-0002-3263-2403

References

[1] Subia B, Kundu J and Kundu S 2010 Biomaterial scaffold fabrication techniques for potential tissue engineering applications *Tissue Engineering* vol 141 (InTechOpen) pp 13–18
[2] Pacheco D P, Vargas N S, Visentin S and Petrini P 2021 From tissue engineering to engineering tissues: the role and application of in vitro models *Biomater. Sci.* **9** 70–83
[3] Li C, Ouyang L, Armstrong J P and Stevens M M 2021 Advances in the fabrication of biomaterials for gradient tissue engineering *Trends Biotechnol.* **39** 150–64
[4] Seidi A, Ramalingam M, Elloumi-Hannachi I, Ostrovidov S and Khademhosseini A 2011 Gradient biomaterials for soft-to-hard interface tissue engineering *Acta Biomater.* **7** 1441–51
[5] Kundu J, Pati F, Hun Jeong Y and Cho D W 2013 *Chapter 2—Biomaterials for Biofabrication of 3D Tissue Scaffolds Biofabrication* ed G Forgacs and W Sun (William Andrew Publishing) pp 23–46
[6] Sun A, He X, Ji X, Hu D, Pan M, Zhang L and Qian Z 2021 Current research progress of photopolymerized hydrogels in tissue engineering *Chin. Chem. Lett.* **32** 2117–26
[7] Randhawa A, Dutta S D, Ganguly K, Patel D K, Patil T V and Lim K 2023 Recent advances in 3D printing of photocurable polymers: types, mechanism, and tissue engineering application *Macromol. Biosci.* **23** 2200278
[8] Xu C, Lee W, Dai G and Hong Y 2018 Highly elastic biodegradable single-network hydrogel for cell printing *ACS Appl. Mater. Interfaces* **10** 9969–79
[9] Sakai S, Kamei H, Mori T, Hotta T, Ohi H, Nakahata M and Taya M 2018 Visible light-induced hydrogelation of an alginate derivative and application to stereolithographic

bioprinting using a visible light projector and acid red *Biomacromolecules* **19** 672–9
[10] Mora-Boza A, Ghebrezadik S G, Leisen J E and García A J 2023 Rapid and Facile Light-Based Approach to Fabricate Protease-Degradable Poly(ethylene glycol)—norbornene Microgels for Cell Encapsulation *Adv. Healthc. Mater.* **12**
[11] Xin S, Wyman O M and Alge D L 2018 Assembly of PEG microgels into porous cell-instructive 3D scaffolds via thiol-ene click chemistry *Adv. Healthcare Mater.* **7** 1800160
[12] Caldwell A S, Aguado B A and Anseth K S 2020 Cell Culture: Designing Microgels for Cell Culture and Controlled Assembly of Tissue Microenvironments *Adv. Healthc. Mater.* **30**
[13] Lowen J M, Bond G C, Griffin K H, Shimamoto N K, Thai V L and Leach J Kent 2023 Multisized Photoannealable Microgels Regulate Cell Spreading, Aggregation, and Macrophage Phenotype through Microporous Void Space *Adv. Healthc. Mater.* **12**
[14] Zhu W, Ma X, Gou M, Mei D, Zhang K and Chen S 2016 3D printing of functional biomaterials for tissue engineering *Curr. Opin. Biotechnol.* **40** 103–12
[15] Kim S H, Yeon Y K, Lee J M, Chao J R, Lee Y J, Seo Y B, Sultan M T, Lee O J, Lee J S and Yoon S 2018 Precisely printable and biocompatible silk fibroin bioink for digital light processing 3D printing *Nat. Commun.* **9** 1620
[16] Mau R, Nazir J, John S and Seitz H 2019 Preliminary study on 3D printing of PEGDA hydrogels for frontal sinus implants using digital light processing (DLP) *Curr. Direction Biomed. Eng.* **5** 249–52
[17] Zanon M, Baruffaldi D, Sangermano M, Pirri C F, Frascella F and Chiappone A 2021 Visible light-induced crosslinking of unmodified gelatin with PEGDA for DLP-3D printable hydrogels *Eur. Polym. J.* **160** 110813
[18] Chang S Y, Ching T and Hashimoto M 2022 Bioprinting using PEGDMA-based hydrogel on DLP printer *Mater. Today Proc.* **70** 179–83
[19] Kadry H, Wadnap S, Xu C and Ahsan F 2019 Digital light processing (DLP) 3D-printing technology and photoreactive polymers in fabrication of modified-release tablets *Eur. J. Pharm. Sci.* **135** 60–67
[20] Preobrazhenskiy I, Tikhonov A, Evdokimov P, Shibaev A and Putlyaev V 2021 DLP printing of hydrogel/calcium phosphate composites for the treatment of bone defects *Open Ceram.* **6** 100115
[21] Griffin D R, Weaver W M, Scumpia P O, Di Carlo D and Segura T 2015 Accelerated wound healing by injectable microporous gel scaffolds assembled from annealed building blocks *Nat. Mater.* **14** 737–44
[22] Meena L K, Rather H, Kedaria D and Vasita R 2019 Polymeric microgels for bone tissue engineering applications–a review *Int. J. Polym. Mater. Polym. Biomater.* **69** 381–97
[23] Ye C *et al* 2021 *Fabricating structured particles through rapid hardening and tailored collection methods*
[24] Nunes J, Tsai S, Wan J and Stone H A 2013 Dripping and jetting in microfluidic multiphase flows applied to particle and fibre synthesis *J. Phys. D: Appl. Phys.* **46** 114002
[25] de Rutte J M, Koh J and Di Carlo D 2019 Scalable high-throughput production of modular microgels for in situ assembly of microporous tissue scaffolds *Adv. Funct. Mater.* **29** 1900071
[26] Ramachandran K and Harrington S M 2017 Microencapsulation technique and products thereof *US Patent* 9642814B2
[27] Harrington S, Ott L, Karanu F, Ramachandran K and Stehno-Bittel L 2021 A versatile microencapsulation platform for hyaluronic acid and polyethylene glycol *Tissue Eng.* A **27** 153–64
[28] Jiang J, Shea G, Rastogi P, Kamperman T, Venner C H and Visser C W 2021 Continuous high-throughput fabrication of architected micromaterials via in-air photopolymerization *Adv. Mater.* **33** 2006336
[29] Drury J L and Mooney D J 2003 Hydrogels for tissue engineering: scaffold design variables and applications *Biomaterials* **24** 4337–51
[30] Zhu J 2010 Bioactive modification of poly(ethylene glycol) hydrogels for tissue engineering *Biomaterials* **31** 4639–56
[31] Elisseeff J, McIntosh W, Anseth K, Riley S, Ragan P and Langer R 2000 Photoencapsulation of chondrocytes in poly (ethylene oxide)-based semi-interpenetrating networks *J. Biomed. Mater. Res.* **51** 164–71
[32] Mironi-Harpaz I, Wang D Y, Venkatraman S and Seliktar D 2012 Photopolymerization of cell-encapsulating hydrogels: crosslinking efficiency versus cytotoxicity *Acta Biomater.* **8** 1838–48
[33] Roberts J J and Bryant S J 2013 Comparison of photopolymerizable thiol-ene PEG and acrylate-based PEG hydrogels for cartilage development *Biomaterials* **34** 9969–79
[34] Ligon-Auer S C, Schwentenwein M, Gorsche C, Stampfl J and Liska R 2016 Toughening of photo-curable polymer networks: a review *Polym. Chem.* **7** 257–86
[35] Yagci Y, Jockusch S and Turro N J 2010 Photoinitiated polymerization: advances, challenges, and opportunities *Macromolecules* **43** 6245–60
[36] Debroy D, Oakey J and Li D 2018 Interfacially-mediated oxygen inhibition for precise and continuous poly (ethylene glycol) diacrylate (PEGDA) particle fabrication *J. Colloid Interface Sci.* **510** 334–44
[37] Huling J, Lyko B, Illner S, Fiedler N, Grabow N and Teske M 2020 Development of UV-reactive electrospinning method based on poly (ethylene glycol) diacrylate crosslinking *Curr. Direction Biomed. Eng.* **6** 189–92
[38] Zou Y, Zhang L, Yang L, Zhu F, Ding M, Lin F, Wang Z and Li Y 2018 "Click" chemistry in polymeric scaffolds: bioactive materials for tissue engineering *J. Control. Release* **273** 160–79
[39] Bagheri A and Jin J 2019 Photopolymerization in 3D printing *ACS Appl. Polym. Mater.* **1** 593–611
[40] McCall J D and Anseth K S 2012 Thiol–ene photopolymerizations provide a facile method to encapsulate proteins and maintain their bioactivity *Biomacromolecules* **13** 2410–7
[41] Xu Z and Bratlie K M 2018 Click chemistry and material selection for in situ fabrication of hydrogels in tissue engineering applications *ACS Biomater. Sci. Eng.* **4** 2276–91
[42] Hoyle C E and Bowman C N 2010 Thiol–ene click chemistry *Angew. Chem., Int. Ed.* **49** 1540–73
[43] Cramer N B, Reddy S K, O'Brien A K and Bowman C N 2003 Thiol— ene photopolymerization mechanism and rate limiting step changes for various vinyl functional group chemistries *Macromolecules* **36** 7964–9
[44] Kim M H and Lin C C 2023 Poly (ethylene glycol)–norbornene as a photoclick bioink for digital light processing 3D bioprinting *ACS Appl. Mater. Interfaces* **15** 2737–46
[45] Yu C, Miller K L, Schimelman J, Wang P, Zhu W, Ma X, Tang M, You S, Lakshmipathy D and He F 2020 A sequential 3D bioprinting and orthogonal bioconjugation approach for precision tissue engineering *Biomaterials* **258** 120294
[46] Dubbin K *et al* 2021 Projection microstereolithographic microbial bioprinting for engineered biofilms *Nano Lett.* **21** 1352–9
[47] Fairbanks B D, Schwartz M P, Bowman C N and Anseth K S 2009 Photoinitiated polymerization of PEG-diacrylate with lithium phenyl-2, 4, 6-trimethylbenzoylphosphinate: polymerization rate and cytocompatibility *Biomaterials* **30** 6702–7
[48] Whelehan M and Marison I W 2011 Microencapsulation using vibrating technology *J. Microencapsul.* **28** 669–88
[49] Serp D, Cantana E, Heinzen C, Von Stockar U and Marison I 2000 Characterization of an encapsulation device for the

production of monodisperse alginate beads for cell immobilization *Biotechnol. Bioeng.* **70** 41–53
[50] Heinzen C, Berger A and Marison I 2004 Use of vibration technology for jet break-up for encapsulation of cells and liquids in monodisperse microcapsules *Fundamentals of Cell Immobilisation Biotechnology* (Springer) pp 257–75
[51] Allevi by 3D Systems 2022 *Live/Dead Quantification Using Fiji - Step-by-Step Guide | Support* (available at: https://www.allevi3d.com/livedead-assay-quantification-fiji/)
[52] Fairbanks B D, Schwartz M, Halevi A E, Nuttelman C R, Bowman C and Anseth K 2009 A versatile synthetic extracellular matrix mimic via thiol-ene photopolymerization *Adv. Mater.* **21** 5005–10
[53] Yeh Y C, Ouyang L, Highley C B and Burdick J A 2017 Norbornene-modified poly (glycerol sebacate) as a photocurable and biodegradable elastomer *Polym. Chem.* **8** 5091–9
[54] Malandrino A, Mak M, Kamm R D and Moeendarbary E 2018 Complex mechanics of the heterogeneous extracellular matrix in cancer *Extrem. Mech. Lett.* **21** 25–34
[55] Ding H, Dong M, Zheng Q and Wu Z L 2022 Digital light processing 3D printing of hydrogels: a minireview *Mol. Syst. Des. Eng.* **7** 1017–29
[56] Malekpour A and Chen X 2022 Printability and cell viability in extrusion-based bioprinting from experimental, computational, and machine learning views *J. Funct. Biomater.* **13** 40
[57] Liz-Basteiro P, Reviriego F, Martínez-Campos E, Reinecke H, Elvira C, Rodríguez-Hernández J and Gallardo A 2023 Vat photopolymerization 3D printing of hydrogels with re-adjustable swelling *Gels* **9** 600
[58] Germain L, Fuentes C A, van Vuure A W, Des Rieux A and Dupont-Gillain C 2018 3D-printed biodegradable gyroid scaffolds for tissue engineering applications *Mater. Des.* **151** 113–22
[59] Torres-Rendon J G, Femmer T, De Laporte L, Tigges T, Rahimi K, Gremse F, Zafarnia S, Lederle W, Ifuku S and Wessling M 2015 Bioactive gyroid scaffolds formed by sacrificial templating of nanocellulose and nanochitin hydrogels as instructive platforms for biomimetic tissue engineering *Adv. Mater.* **27** 2989–95
[60] Mohanty A K, Datta A and Venkatraj V 2013 A model for cancer tissue heterogeneity *IEEE Trans. Biomed. Eng.* **61** 966–74
[61] Liu C, Li M, Dong Z X, Jiang D, Li X, Lin S, Chen D, Zou X, Zhang X D and Luker G D 2021 Heterogeneous microenvironmental stiffness regulates pro-metastatic functions of breast cancer cells *Acta Biomater.* **131** 326–40
[62] Tellez-Gabriel M, Ory B, Lamoureux F, Heymann M F and Heymann D 2016 Tumour heterogeneity: the key advantages of single-cell analysis *Int. J. Mol. Sci.* **17** 2142
[63] Bjugstad K, Redmond D Jr, Lampe K, Kern D, Sladek J Jr and Mahoney M 2008 Biocompatibility of PEG-based hydrogels in primate brain *Cell Transplant.* **17** 409–15
[64] Escudero-Castellanos A, Ocampo-García B E, Domínguez-García M V, Flores-Estrada J and Flores-Merino M V 2016 Hydrogels based on poly (ethylene glycol) as scaffolds for tissue engineering application: biocompatibility assessment and effect of the sterilization process *J. Mater. Sci., Mater. Med.* **27** 1–10
[65] El-Sherbiny I M and Yacoub M H 2013 Hydrogel scaffolds for tissue engineering: progress and challenges *Glob. Cardiol. Sci. Pract.* **2013** 38
[66] Zuidema J M, Rivet C J, Gilbert R J and Morrison F A 2014 A protocol for rheological characterization of hydrogels for tissue engineering strategies *J. Biomed. Mater. Res.* B **102** 1063–73
[67] Vanderhooft J L, Alcoutlabi M, Magda J J and Prestwich G D 2009 Rheological properties of cross-linked hyaluronan–gelatin hydrogels for tissue engineering *Macromol. Biosci.* **9** 20–28
[68] Gao X, He C, Xiao C, Zhuang X and Chen X 2013 Biodegradable pH-responsive polyacrylic acid derivative hydrogels with tunable swelling behavior for oral delivery of insulin *Polymer* **54** 1786–93
[69] Pacelli S, Paolicelli P, Avitabile M, Varani G, Di Muzio L, Cesa S, Tirillò J, Bartuli C, Nardoni M and Petralito S 2018 Design of a tunable nanocomposite double network hydrogel based on gellan gum for drug delivery applications *Eur. Polym. J.* **104** 184–93
[70] Williams C G, Malik A N, Kim T K, Manson P N and Elisseeff J H 2005 Variable cytocompatibility of six cell lines with photoinitiators used for polymerizing hydrogels and cell encapsulation *Biomaterials* **26** 1211–8
[71] Holmes R, Yang X B, Dunne A, Florea L, Wood D and Tronci G 2017 Thiol-ene photo-click collagen-PEG hydrogels: impact of water-soluble photoinitiators on cell viability, gelation kinetics and rheological properties *Polymers* **9** 226
[72] Xu H, Casillas J, Krishnamoorthy S and Xu C 2020 Effects of Irgacure 2959 and lithium phenyl-2, 4, 6-trimethylbenzoylphosphinate on cell viability, physical properties, and microstructure in 3D bioprinting of vascular-like constructs *Biomed. Mater.* **15** 055021
[73] Duong V T and Lin C 2023 Digital light processing 3D bioprinting of gelatin-norbornene hydrogel for enhanced vascularization *Macromol. Biosci.* **23** 2300213
[74] Mazzoccoli J P, Feke D L, Baskaran H and Pintauro P N 2010 Mechanical and cell viability properties of crosslinked low-and high-molecular weight poly (ethylene glycol) diacrylate blends *J. Biomed. Mater. Res.* A **93** 558–66
[75] Brandenberger H, Nüssli D, Piech V and Widmer F 1999 Monodisperse particle production: a method to prevent drop coalescence using electrostatic forces *J. Electrost.* **45** 227–38
[76] Visser C Willem, Kamperman T, Karbaat L P, Lohse D and Karperien M 2018 In-air microfluidics enables rapid fabrication of emulsions, suspensions, and 3D modular (bio)materials *Sci. Adv.* **4** eaao1175
[77] van Loo B, Schot M, Gurian M, Kamperman T and Leijten J 2024 Single-step biofabrication of in situ spheroid-forming compartmentalized hydrogel for clinical-sized cartilage tissue formation *Adv. Healthcare Mater.* **13** 2300095
[78] van Loo B *et al* 2023 Mass production of lumenogenic human embryoid bodies and functional cardiospheres using in-air-generated microcapsules *Nat. Commun.* **14** 6685
[79] Jiang Z, Xia B, McBride R and Oakey J 2017 A microfluidic-based cell encapsulation platform to achieve high long-term cell viability in photopolymerized PEGNB hydrogel microspheres *J. Mater. Chem.* B **5** 173–80
[80] Lin C, Ki C S and Shih H 2015 Thiol–norbornene photoclick hydrogels for tissue engineering applications *J. Appl. Polym. Sci.* **132** 41563
[81] Göckler T, Haase S, Kempter X, Pfister R, Maciel B R, Grimm A, Molitor T, Willenbacher N and Schepers U 2021 Tuning superfast curing thiol-norbornene-functionalized gelatin hydrogels for 3D bioprinting *Adv. Healthcare Mater.* **10** 2100206
[82] Kamperman T, Henke S, van den Berg A, Shin S R, Tamayol A, Khademhosseini A, Karperien H B J and Leijten J C H 2017 Single cell microgel based modular bioinks for uncoupled cellular micro-and macrenvironments *Adv. Healthcare Mater.* **6** 1600913
[83] Husman D, Welzel P B, Vogler S, Bray L J, Träber N, Friedrichs J, Körber V, Tsurkan M V, Freudenberg U and Thiele J 2020 Multiphasic microgel-in-gel materials to recapitulate cellular mesoenvironments in vitro *Biomater. Sci.* **8** 101–8

[84] Li M, van Zee M, Riche C T, Tofig B, Gallaher S D, Merchant S S, Damoiseaux R, Goda K and Di Carlo D 2018 A gelatin microdroplet platform for high-throughput sorting of hyperproducing single-cell-derived microalgal clones *Small* **14** 1803315
[85] Varma A, Gemeda H B, McNulty M J, McDonald K A, Nandi S and Knipe J M 2021 Immobilization of transgenic plant cells towards bioprinting for production of a recombinant biodefense agent *Biotechnol. J.* **16** 2100133
[86] Brewer A, Dohnalkova A, Shutthanandan V, Kovarik L, Chang E, Sawvel A M, Mason H E, Reed D, Ye C and Hynes W F 2019 Microbe encapsulation for selective rare-earth recovery from electronic waste leachates *Environ. Sci. Technol.* **53** 13888–97